Structural Engineering and Mechanics, Vol. 24, No. 3 (2006)323-337
DOI: http://dx.doi.org/10.12989/sem.2006.24.3.323

Simulations of the hysteretic behavior of thin-wall cold-formed steel members under cyclic uniaxial loading

Jun Dong†

Research Institute of Steel Structures, Nanjing University of Technology, Nanjing, 210009, China

Shiqi Wang‡

Metallurgical Design Institute of Shandong Province, Jinan, 250014, China

Xi Lu‡†

Research Institute of Steel Structures, Nanjing University of Technology, Nanjing, 210009, China

(Received May 13, 2005, Accepted May 8, 2006)

Abstract. In this paper, the hysteretic behaviors of channel and C-section cold-formed steel members (CFSMs) under cyclic axial loading were simulated with the finite element method. Geometric and material nonlinearities, Bauschinger effect, strain hardening and strength improvement at corner zones were taken into account. Extensive numerical results indicated that, as the width-to-thickness ratio increases, local buckling occurs prematurely. As a result, the hysteretic behavior of the CFSMs degrades and their energy dissipation capability decreases. Due to the presence of lips, the hysteretic behavior of a C-section steel member is superior to that of its corresponding channel section. The intermediate stiffeners in a C-section steel member postpone the occurrence of local buckling and change its shapes, which can greatly improve its hysteretic behavior and energy dissipation capability. Therefore, the CFSMs with a large width-to-thickness ratio can be improved by adding lips and intermediate stiffeners, and can be used more extensively in residential buildings located in seismic areas.

Keywords: hysteretic behavior; thin-wall cold-formed steel members; cyclic loading; finite element method; cold-formed steel framed residence.

1. Introduction

Various cross-sectional configurations can be economically produced in cold-formed steel members (CFSMs) by cold-forming operations (Yu 2000). Compared with hot rolled steels, cold-formed steel has larger width-to-thickness and strength-to-weight ratios. As a result, CFSMs have

† Professor, Ph.D., Corresponding author, E-mail: djdongjun@263.net
‡ Engineer
‡† Postgraduate Student

been widely utilized as main structural members in low-rise cold-formed steel framed residential buildings. At present, research on the CFSMs is mainly focused on the range of elastic and static performance; the post-buckling hysteretic behavior of the CFSMs has not been investigated extensively. Since residential buildings in many parts of China are required to be strengthened for seismic loads, and in most cases, cold-formed steel framed structures are preferred, the hysteretic behavior of the CFSMs must be further investigated. Due to the complexity in their cross-section configurations, geometric and material nonlinearities, initial geometric imperfection, cold-forming effect and other factors, the research on the CFSMs often warrants laboratory experimentations. Finite element analysis is, however, more convenient and economical as compared to physical experiments. Thus, using the finite element method to study the hysteretic behavior of the CFSMs before any physical testing is necessary (Banno *et al.* 1998, Goto *et al.* 1998, Ucak and Tsopelas 2004). This paper uses shell element (S4R) and the linear kinematic hardening model to simulate geometric and material nonlinearities through the finite element analysis program ABAQUS V6.4-1 under cyclic uniaxial loading. Bauschinger effect and the effects of strain hardening and strength improvement at the corner zone of cold-formed channels and intermediate stiffened C-section steel members under cyclic uniaxial loading, and the width-to-thickness ratio, the lip and the intermediate stiffener on the hysteretic behavior will be considered.

2. Development of finite element model

In order to take into account the effect of the width-to-thickness ratio, the lip and the intermediate stiffener on the hysteretic behavior of the CFSMs, a general purpose finite element nonlinear analysis program ABAQUS V6.4-1 was used to simulate the hysteretic behavior of the CFSMs subjected to cyclic uniaxial loading. Followings are the specific descriptions of material hardening model, model sizes and finite element mesh and boundary condition.

2.1 Material hardening model

In order to simulate the Bauschinger effect of the CFSMs under cyclic uniaxial loading, the linear kinematic hardening model with constant hardening modulus was used in the finite element method analysis (Banno *et al.* 1998). The linear kinematic hardening model is a simplified model for the Bauschinger effect. When the stress varies from uniaxial tension to uniaxial compression, the increment of tension stress equals to the decrement of compression stress; the range of tension and compression stresses always equals 2 times the yield stress. Hence, the center of the yield surface shifts in stress space (kinematic hardening behavior) and its size and shape is constant (the Bauschinger effect).

Due to the cold-forming effect, the corner zone and the flat zone of cross-section should be simulated in the finite element model, as shown in Fig. 1. In the corner zone, the cold-forming effect on strength improvement can be determined from the Canadian Standards for Cold-Formed Steel Structural Members (Canadian Standards Association 1994):

$$\sigma_y' = \sigma_y + \frac{5D}{W^*}(\sigma_u - \sigma_y) \tag{1}$$

where σ_y' is the average tensile yield strength over the entire cross section; D is the multiple of a

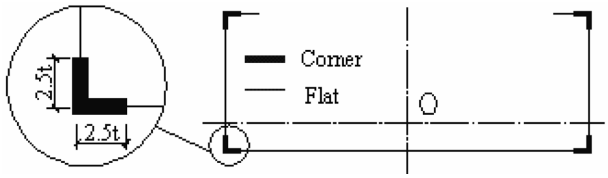

Fig. 1 Definition of the corner zone and the flat zone of cross-section

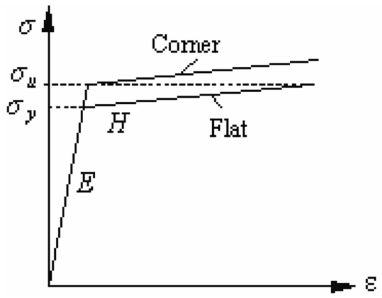

Fig. 2 Ideal stress-strain curves

right angle that is equal to the value gained from the sum of the bend angles divided by 90; W^* is the ratio of the total centerline length l to thickness t in the cross-section of the steel members. Eq. (1) can thus be rewritten as:

$$\sigma_y' = \sigma_y + \frac{5D}{W^*}(\sigma_u - \sigma_y) = \sigma_y + \frac{5D}{l/t}(\sigma_u - \sigma_y) = \frac{l - 5Dt}{l}\sigma_y + \frac{5Dt}{l}\sigma_u \quad (2)$$

According to Eq. (2), the cold-forming effect can be considered when the yield stress over two equal distances of 2.5 t each at any right angle, as indicated in Fig. 1, is replaced by the ultimate stress (σ_u). The material chosen in this study is the hot-dip galvanizing cold-formed thin-wall steel of grade Q235 with Young's modulus $E = 206 \times 10^3$ N/mm^2, yield stress $\sigma_y = 235$ N/mm^2, Poisson's ratio $\nu = 0.3$, ultimate tensile stress $\sigma_u = 270$ N/mm^2 N/mm^2, hardening modulus $H = E/100 = 2060$ N/mm^2. The stress-strain relation curves at the corner zone and the flat zone of a cross section are shown in Fig. 2 (Peng 2004).

2.2 Model sizes

To prevent the overall buckling mode of a compression member, the length of the member (L) should be less than 20 times the minimum radius of gyration of the cross-section ($20i_{\min}$). On the other hand, to minimize the end effect, the length of the member should be more than 3 times the maximum width of the cross-section ($3d$) (Abdel-Rahman and Sivakumaran 1998, Tang *et al.* 1998). For all finite element models in this study, the length of the member was considered to be $3d$, which meets the two requirements mentioned above. The finite element model of singly symmetric channel, C- and intermediate stiffened C-section steel members was used to analyze the effect of the width-to-thickness ratio, the lip, and the intermediate stiffener on their hysteretic behavior. The specific model sizes and configurations of the cross-section are given in Table 1 and Fig. 3, respectively. The first one or two upper case letters "Cxxyy", "CLxxyy" and "CLxxyySz" designate a channel section, a C-section, and an intermediate stiffened C-section, respectively; the following two digits "xx" indicate the width-to-thickness ratio of the webs, the succeeding two digits "yy" represent the width-to-thickness ratio of the flanges, the seventh letter "S" for the stiffened C-section symbolizes the presence of stiffeners, and the last digit "z" means the number of the intermediate stiffeners of the webs. For the cross section shown in Figs. 3(c), (d), a subelement was introduced for each portion of the cross section between two adjacent stiffeners, between the web and the intermediate stiffener or between one edge and the intermediate stiffener.

Table 1 Model sizes (all units in mm except as noted)

Designation	Height w	Width b	Web's stiffer	Web's flat	Flange's stiffer	Flange's flat	Lip a	Thickness T	Area A(mm^2)	Center x	Length L
C2010	60	30	—	—	—	—	—	3	360	7.50	180
C4015	120	45	—	—	—	—	—	3	630	9.64	360
C6525	195	75	—	—	—	—	—	3	1035	16.30	585
CL2010	60	30	—	—	—	—	9	3	414	10.43	180
CL4015	120	45	—	—	—	—	15	3	720	14.06	360
CL6525	195	75	—	—	—	—	24	3	1179	23.47	585
CL4015S1	120	45	30	45	/	/	15	3	810	15.39	360
CL6525S1	195	75	45	75	/	/	24	3	1314	25.07	585
CL6525S2	195	75	30	45	/	/	24	3	1359	23.81	585
CL10540S2	315	120	45	75	30	45	15	3	2295	35.17	945

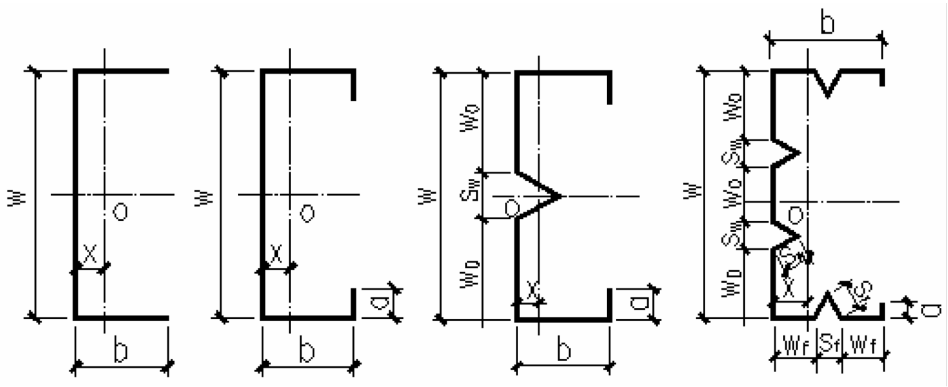

(a) Cxxyy (b) CLxxyy (c) CLxxyyS1 (d) CLxxyyS2

Fig. 3 Configuration of cross-sections

2.3 Finite element mesh and boundary condition

The fixed-end boundary condition of the bottom end of an axial member was introduced by restraining all degrees of freedom at both ends of a 3-D rigid element R3D4 except for the axial deformation at the top end of the element. In consideration of the computational efficiency and analysis accuracy, different mesh sizes were utilized for the flat zone and the corner zone, respectively. For channel CFSMs, the web was divided into 12 segments and the flange was divided into 6 segments; for C-section CFSMs, the web was also divided into 12 segments, the flange was divided into 6 segments, and the lip was divided into 2 segments. For the intermediate stiffened C-section CFSMs, the web's stiffer was divided into 3 segments (30 mm) or 4 segments (45 mm), the web's flat was divided into 4 segments (45 mm) or 6 segments (75 mm), the flange's stiffer was divided into 3 segments, the flange's flat was divided into 4 segments and the lip was divided into 2 segments.

Table 2 Dimensions and material properties of test specimens

Specimen	b (mm)	d (mm)	t (mm)	L (mm)	Young's modulus N/mm^2	Yield stress N/mm^2	Ultimate stress N/mm^2	Strain hardening modulus N/mm^2	Poisson's ratio
P40	262.8	234.7	5.71	1340	2.09×10^5	310	443	2.24×10^3	0.251
P60	382.6	354.2	5.97	1640	2.09×10^5	310	443	2.24×10^3	0.251

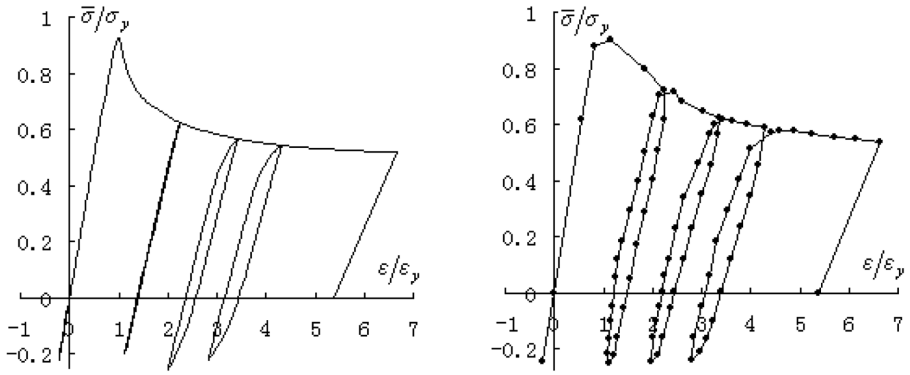

(a) Computational results (b) Test data

Fig 4 Hysteretic curves of short column P40 under cyclic uniaxial loading

3. Finite element analysis

3.1 Validity of the finite element model

In order to verify the validity of the finite element model, the test results of box-section short columns with a large width-to-thickness ratio under cyclic uniaxial loading by Fukumoto and Kusama (1985) were used (Fukumoto and Kusama 1985). The cross-section dimensions and material properties of the test specimens are given in Table 2.

The hysteretic curves of the short columns are shown in Figs. 4 and 5, in which the dotted lines represent the test data and the solid lines the numerical results from the finite element models. In these figures, both stress and stain are defined to be positive in compression and negative in tension, $\bar{\sigma}$ and $\bar{\varepsilon}$ are the average stress and strain ($\bar{\sigma} = N/A$, N is the axial load and A is the cross-section area; $\bar{\varepsilon} = \delta/L$, δ is the axial displacement of the member and L is the length of the member), σ_y and ε_y are the yield stress and yield strain, respectively ($\varepsilon_y = \sigma_y/E$, E is the Young's modulus).

By comparing Fig. 4 with Fig. 5, it can be observed that the simulated hysteretic curves from the finite element model agree well with those of the test specimens, indicating that the finite element model is quite accurate. The validated finite element model established by the above method will be applied to the following analysis for the hysteretic behavior of the CFSMs under cyclic uniaxial loading.

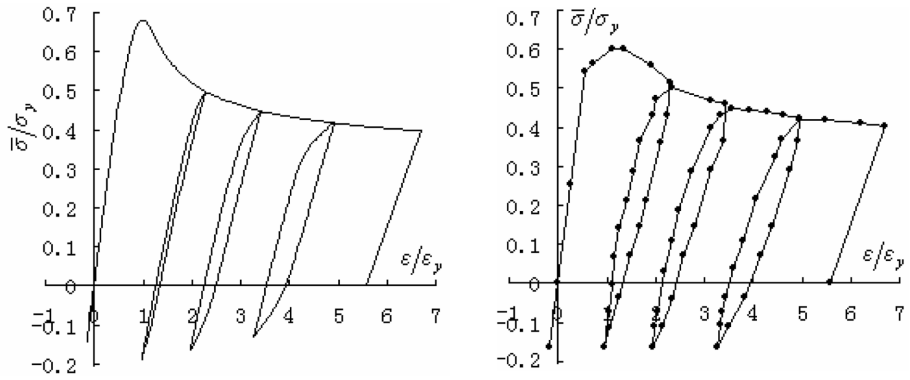

(a) Computational results (b) Test data

Fig 5 Hysteretic curves of short column P60 under cyclic uniaxial loading

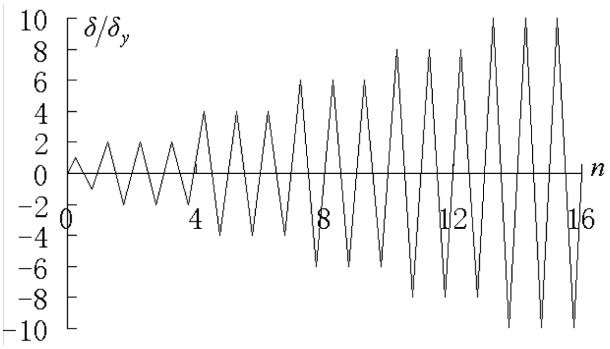

Fig 6 Loading pattern

3.2 Loading pattern

The cyclic uniaxial loading was applied with incrementally increasing controlled displacements in the following analysis. The load protocol is shown in Fig. 6, in which three cycles are repeated at each level except for the initial yield displacement. The displacement sequence is δ_y, $2\delta_y$, $4\delta_y$, $6\delta_y$, $8\delta_y$ and $10\delta_y$.

3.3 Effect of initial imperfection

The effect of initial geometric imperfection was examined both at global and local levels. In what follows, the hysteretic behaviors of the CFSMs were simulated with comparative analyses using the finite element models with no initial geometric imperfection, with global or local geometric imperfections, respectively. According to the Technical Code of Cold-Formed Thin-Wall Steel Structures (GB50018-2002), the global initial geometric imperfection can be considered by assuming a half sine wave of distortion with an amplitude of $L/750$ at the mid height of the column as illustrated in Fig. 7. In this case, the geometric imperfection amplitude δ can be expressed as $\delta = (L/750)\sin(z\pi/L)$ $(0 \le z \le L)$, in which L is the length of the member and z is the z-axis

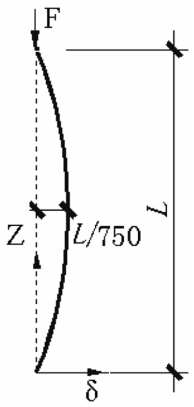

Fig. 7 Global initial geometric imperfection

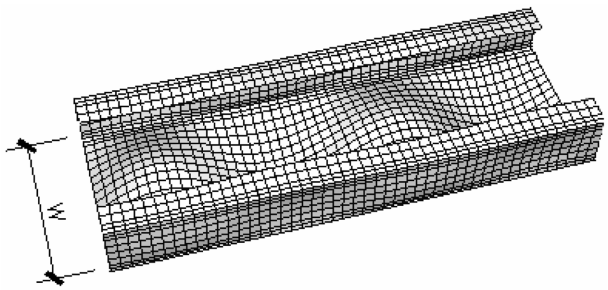

Fig. 8 Local initial geometric imperfection

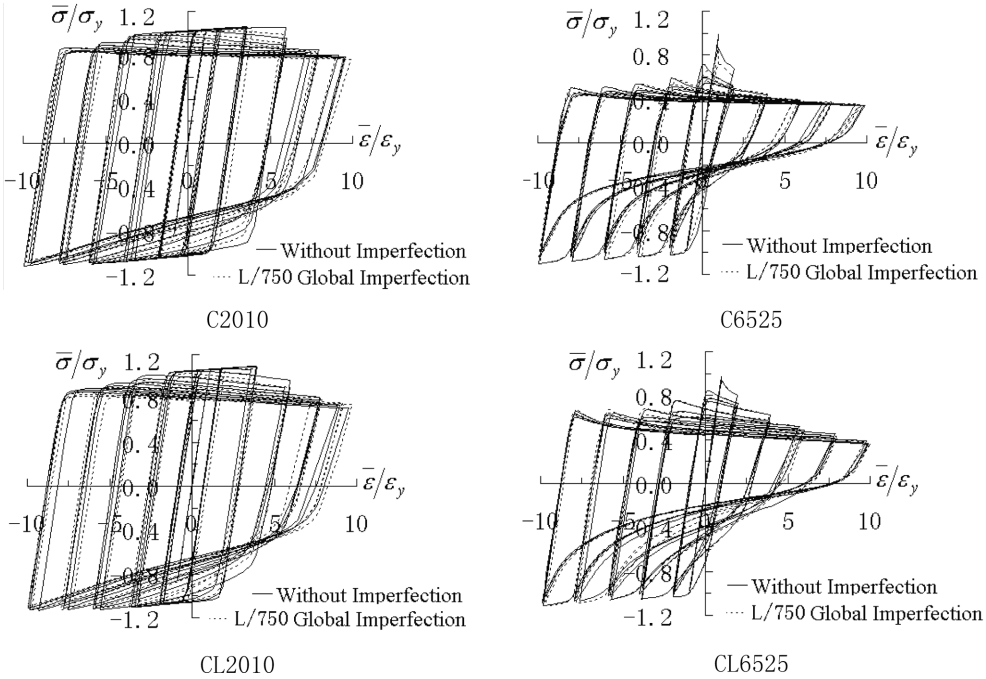

Fig. 9 Effect of global initial geometric imperfection

coordinate of the point of interest. Similarly, the local initial geometric imperfection of a column was considered as the first buckling mode of its elastic buckling analysis (Yong and Yan 2002). The imperfection amplitude equals to the product of the computed local geometric imperfection and $w/150$, in which w is the width of the web as indicated in Fig. 8.

The channel and C-section CFSMs with the maximum and minimum width-to-thickness were analyzed in this study. Their numerical results with and without imperfections are presented in Figs. 9 and 10.

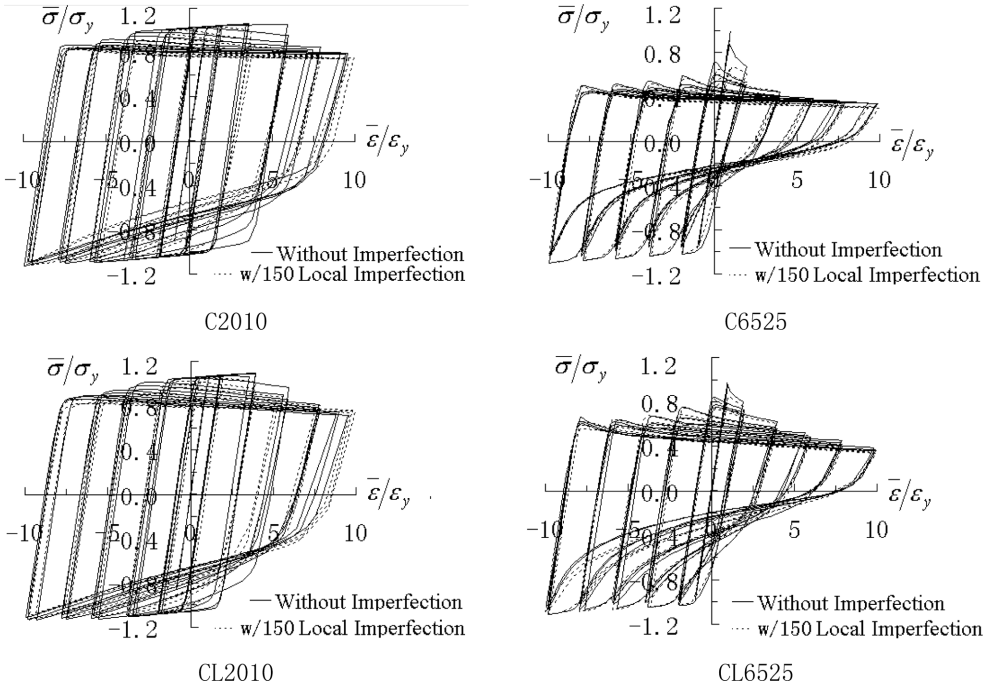

Fig. 10 Effect of local initial geometric imperfection

It can be observed from Figs. 9 and 10 that the global and local initial geometric imperfections decrease the initial maximum compressive load and do not significantly affect the remaining portion of hysteretic curves. Hence the initial geometric imperfection can not be well simulated with the finite element models of the cold-formed steel short columns.

The past investigations (Banno *et al.* 1998, Mamaghani *et al.* 1996) indicated that the residual stress has little effect on the hysteretic behavior of CFSMs. In addition, the distribution of the residual stress is very complicated in numerical simulations. Due to limited space, the effect of residual stress is not considered here.

3.4 Analysis of results

The hysteretic curves of the cold-formed thin-wall channel, C- and intermediate stiffened C-section steel members under cyclic uniaxial loading are summarized in Fig. 11. The solid and dashed lines in the figures denote the results under cyclic and monotonic loading, respectively.

The envelope curves of channel, C- and intermediate stiffened C-section CFSMs are compared in Fig. 12 for various width-to-thickness ratios. To approximately evaluate the seismic performance of CFSMs under cyclic loading, the ratio of energy dissipation ξ and the energy dissipation per volume μ_w are introduced. As illustrated in Fig. 13, the ratio of energy dissipation ξ is defined as the ratio of the envelope area of a simulated hysteretic curve to that of its corresponding ideal elastic-plastic hysteretic curve. That is,

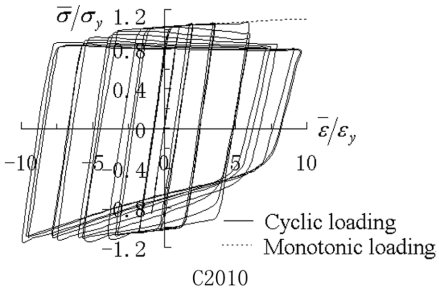

C2010

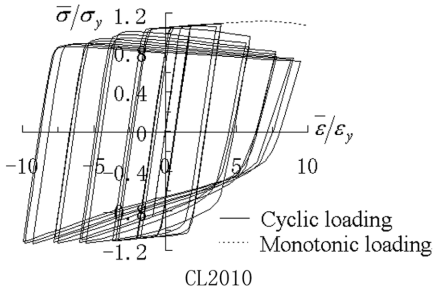

CL2010

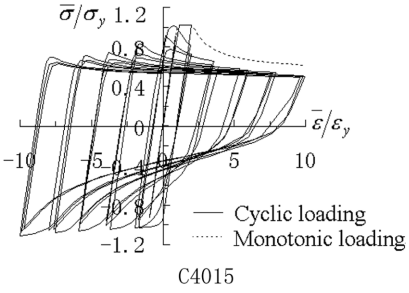

C4015

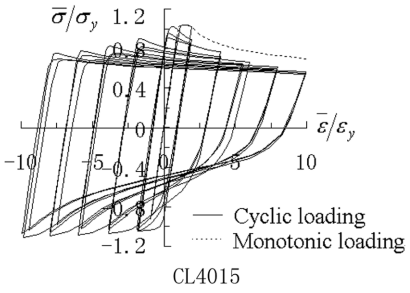

CL4015

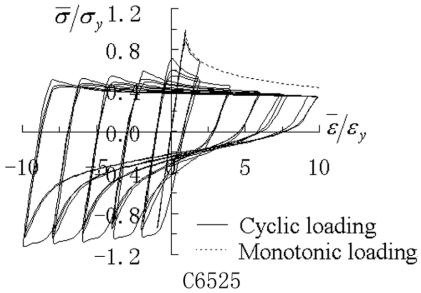

C6525

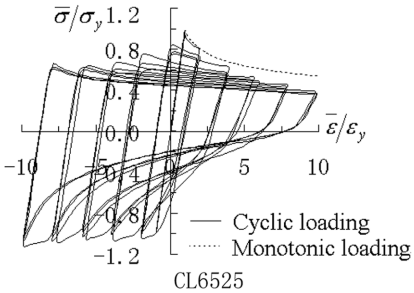

CL6525

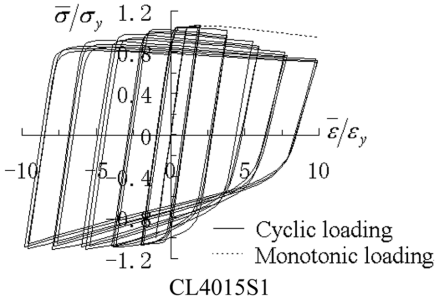

CL4015S1

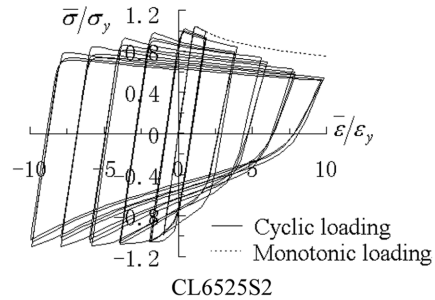

CL6525S2

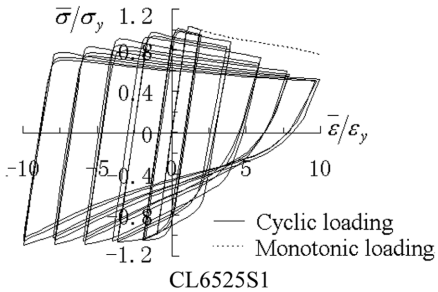

CL6525S1

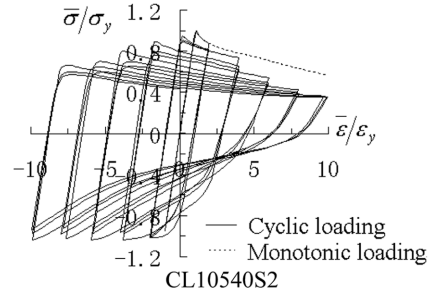

CL10540S2

Fig. 11 Hysteretic curves of the CFSMs

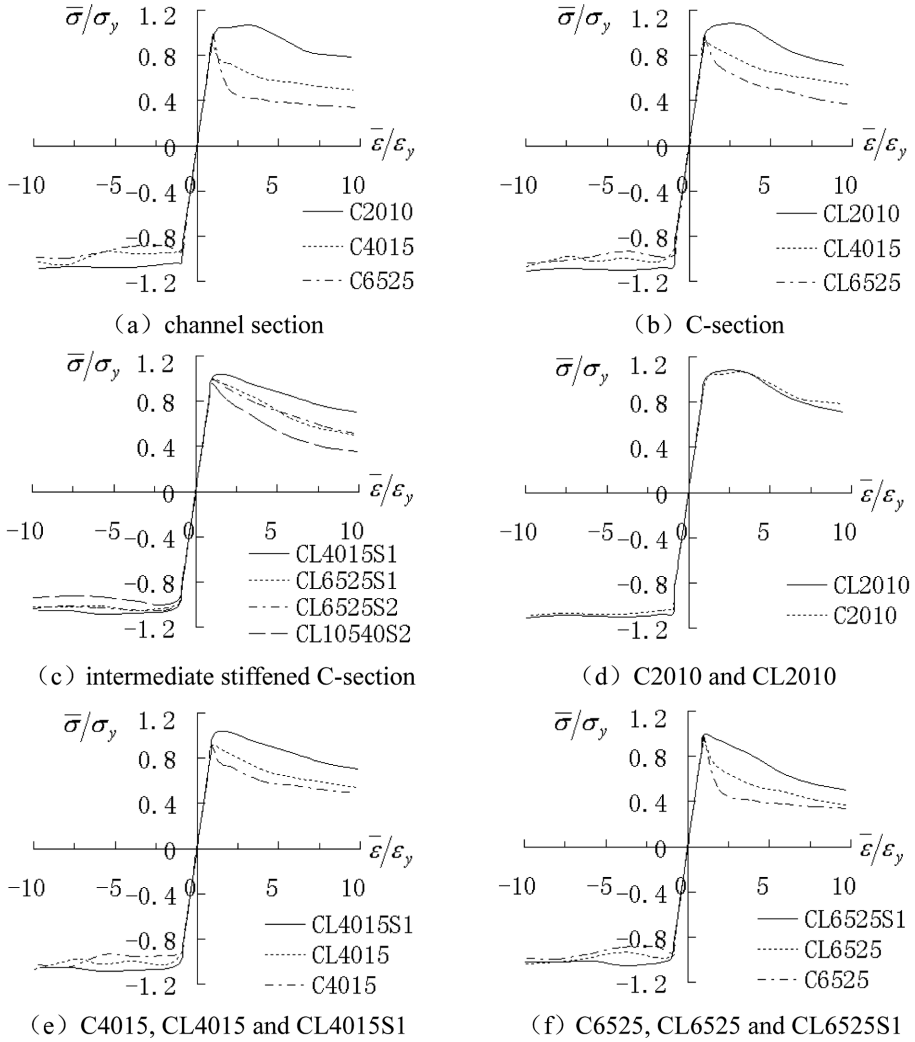

(a) channel section (b) C-section

(c) intermediate stiffened C-section (d) C2010 and CL2010

(e) C4015, CL4015 and CL4015S1 (f) C6525, CL6525 and CL6525S1

Fig. 12 Envelope curves of the hysteretic curves

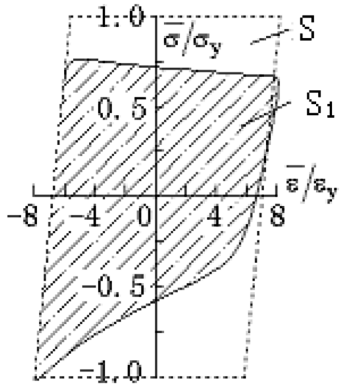

Fig. 13 Envelope area for hysteretic curves

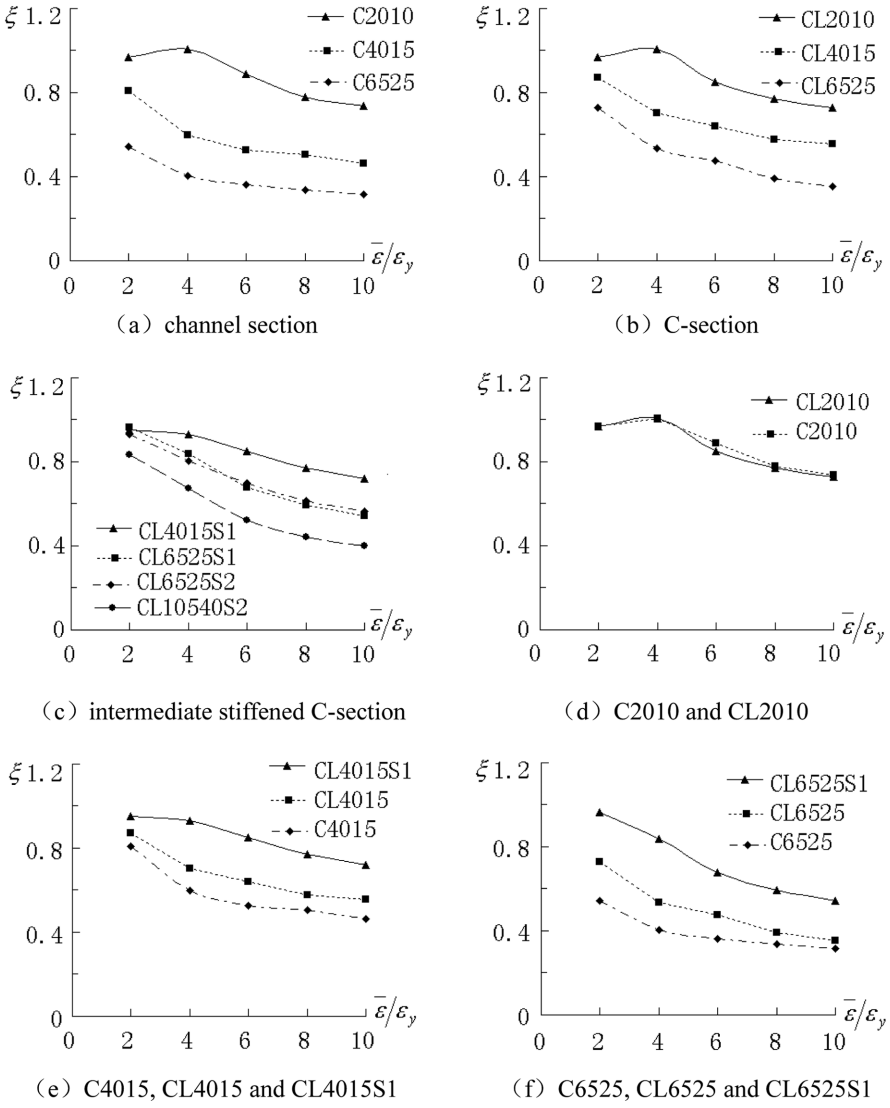

(a) channel section (b) C-section

(c) intermediate stiffened C-section (d) C2010 and CL2010

(e) C4015, CL4015 and CL4015S1 (f) C6525, CL6525 and CL6525S1

Fig 14 Relationship curves between energy dissipation ratio ξ and cyclic strain amplitude

$$\xi = \frac{S_1}{S} \tag{3}$$

where S_1 is the envelope area for the hysteretic curves of a CFSM, and S is the envelope area for its corresponding ideal elastic-plastic hysteretic curve. The energy dissipation per volume μ_w is defined as the ratio of the total energy that the member absorbs in one cycle to the volume of the member:

$$\mu_w = \frac{W}{V} \tag{4}$$

where W is the total energy in one cycle and V is the volume of the member. The relationship among ξ, μ_w, and cyclic strain amplitude are shown in Figs. 14 and 15, respectively.

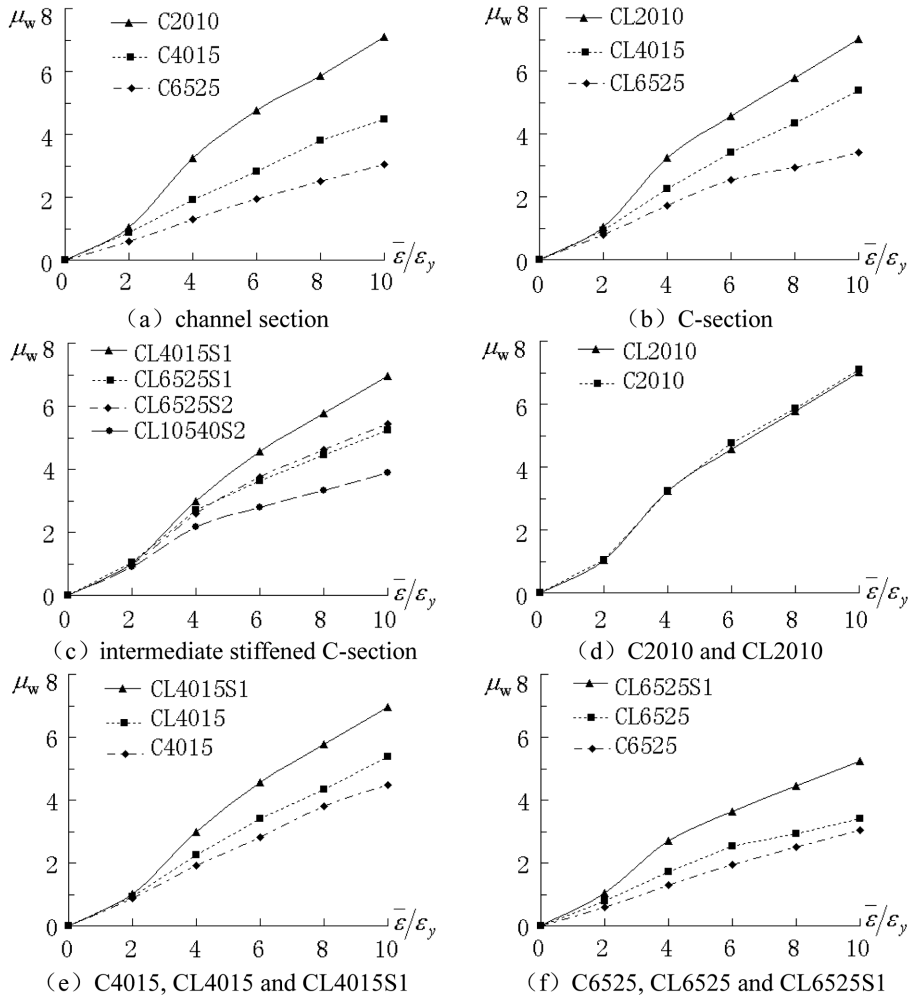

Fig. 15 Relationship curves between energy dissipation per volume μ_w and cyclic strain amplitude

Based on the results presented in Figs. 11-15, the following observations can be made:

1) The basic rules and characters of the hysteretic curves of channel, C- and intermediate stiffened C-section CFSMs are the same, as indicated in Figs. 11 and 12. For instance, the strength of CFSMs under cyclic loading is lower than that under monotonic loading. As the width-to-thickness ratio of the web of CFSMs increases, the hysteretic curves of the CFSMs become leaner and their envelope curves drop rapidly after the initial maximum stress. Consequently, their hysteretic behaviors seriously deteriorate. The reason for this phenomenon is that the increase of the width-to-thickness of the CFSMs leads to local buckling prematurely.
2) When the channel is compared with C-section CFSMs as shown in Figs. 11 and 12, their hysteretic curves are basically the same at a small width-to-thickness ratio of their web. With the increase of the width-to-thickness ratio of their webs, the hysteretic curve of channel section CFSMs is leaner and their capability of energy dissipation decreases rapidly as indicated in Figs. 14 and 15. However, the energy dissipation of C-section CFSMs slowly decreases.

Consequently, at a large web's width-to-thickness ratio, the hysteretic behavior of C-section CFSMs is superior to that of channel CFSMs. For instance, when the web's width-to-thickness ratio of C-section CFSMs equals to 20, the lip does not significantly affect the hysteretic curves. When it is increased to 40, the lip obviously affects the hysteretic curves. When $\overline{\varepsilon}/\varepsilon_y = 10$, $\overline{\sigma}/\sigma_y$ is increased by 10%, and both ξ and μ_w are increased by 20%.

3) As indicated in Figs. 11 and 12, the intermediate stiffener improves the hysteretic behavior of C-section CFSMs. Therefore, the hysteretic curves of the CFSMs with the intermediate stiffener are plumper than that of C-section CFSMs. When the web's width-to-thickness ratio of intermediate stiffened C-section CFSMs equals 40 and $\overline{\varepsilon}/\varepsilon_y = 10$, $\overline{\sigma}/\sigma_y$ is increased by 31%, and ξ and μ_w are increased by 29% as indicated in Figs. 14 and 15. Thus, it can be seen that the intermediate stiffener restrains the local buckling, altering the shape of and postponing the local buckling.
4) Compared with C6525S1 at $\overline{\varepsilon}/\varepsilon_y = 10$, $\overline{\sigma}/\sigma_y$ of C6525S2 was increased by 3% as indicated in Figs. 11 and 12, and ξ and μ_w was increased by 4% as shown in Figs. 14 and 15. These results are consistent with the published results in the literature. That is when the flat width-to-thickness ratio of the subelement is less than 25 and the intermediate stiffener is adequately stiffened, the flat width-to-thickness ratio of the subelement does have an effect on the hysteretic behavior of the intermediate stiffened C-section CFSMs.
5) According to the relationship between energy dissipation ratio, energy dissipation per volume, and cyclic strain amplitude as shown in Figs. 14 and 15, the increase of the web's width-to-thickness ratio for all the CFSMs decreases both the energy dissipation per volume and the energy dissipation ratio. However, as the cyclic strain amplitude increases, the energy dissipation per volume linearly increases. The energy dissipation ratio continue to decrease.

The first bulking modes for various cross-sectional shapes used in this study are shown in Fig. 16. Fig. 16 indicates that the lips and intermediate stiffeners have a significant effect on the buckling shapes. If the member has no lips, the flanges buckled (C6525 vs CL6525). With appropriate intermediate stiffeners, however, when the width-to-thickness ratios of the subelements of

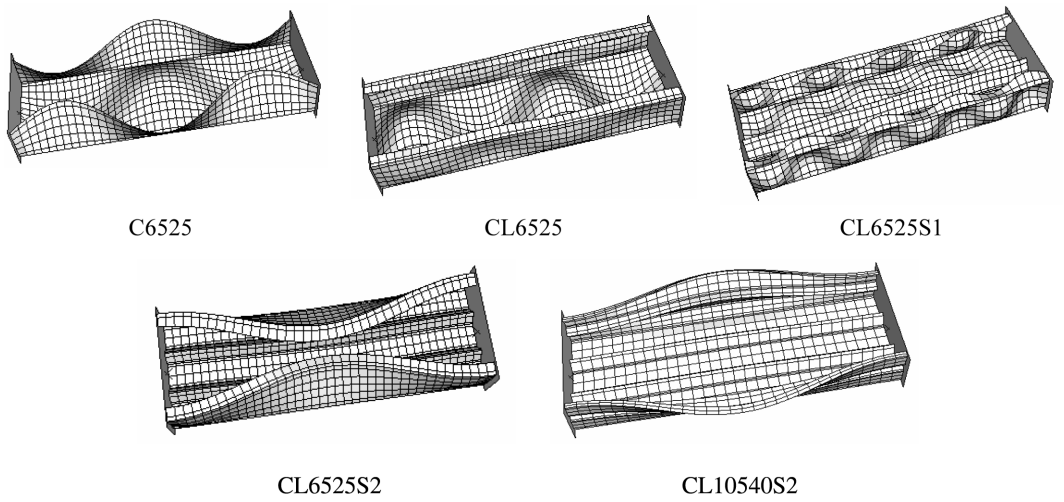

Fig. 16 The first buckling modes

CL6525S1's web approached to the flanges', the member buckled with more half-sine waves, meaning a larger load capacity. The same situation occurred in CL10540S2, because it's lips were too small. Thus, the lips must be logically sized and the intermediate stiffeners must be accurately disposed in order to maximize the carrying capacity of the member.

4. Conclusions

Based on extensive simulations and validations with experimental data, the hysteretic behavior of CFSMs can be predicted efficiently, economically, and accurately using the nonlinear finite element method. The width-to-thickness ratio of the web of CFSMs does significantly affect their hysteretic behavior. The premature failure in local buckling is the primary reason for the deterioration of the hysteretic curves of the CFSMs. For a cold-formed steel member of a large width-to-thickness ratio, the lip and the intermediate stiffener postpone the occurrence of local buckling and alter the shapes of the local buckling, thus improving the hysteretic behavior. Therefore, the width-to-thickness ratio of the web can be controlled in a certain range by the lip and the intermediate stiffener, which promotes the application of CFSMs in the seismic design and retrofit of cold-formed steel framed residential buildings. Special design criterions in this application are yet to be developed with further studies.

Acknowledgements

Financial supports to complete this study were provided in part by the Jiangsu Province Science Foundation Project (BK2005116), the Tenth Five-Year Plan National Science and Technology Problems (2002 BA806B-4), and the Keynote Subject Item of Shanghai Need to Solve "Static-Dynamic Nonlinear Theory, Key Technological Study and its Industrialization for Modern Building Steel Structures".

References

ABAQUS. Inc. (2003), *ABAQUS V6.4-1 Analysis User's Manual.*

Abdel-Rahman, N. and Sivakumaran, K.S. (1998), "A finite element analysis model for the behavior of cold-formed steel members", *Thin-walled Structures*, **31**, 305-324.

Banno, S., Mamaghani, I.H.P., Usami, T. and Mizuno, E. (1998), "Cyclic elastoplastic large deflection analysis of thin steel plates", *J. Eng. Mech.*, **124**(4), 363-370.

Canadian Standards Association (1994), *Cold-Formed Steel Structural Members*, CAN3-S136-M94.

Fukumoto, Y. and Kusama, H. (1985), "Local instability tests of plate elements under cyclic uniaxial loading", *J. Struct. Eng.,* **111**(5), 1051-1067.

GB50018-2002. *Technical Code of Cold-formed Thin-wall Steel Structures.*

Goto, Yoshiaki, Wang, Qingyun and Obata, Makoto (1998), "FEM analysis for hysteretic behavior of thin-walled columns", *J. Struct. Eng.*, **124**(11), 1290-1301.

Mamaghani, I.H.P., Usami, T. and Mizuno, E. (1996), "Inelastic large deflection analysis of structural steel members under cyclic loading", *Eng. Struct.*, **18**(9), 659-668.

Peng, Yapei (2004), "Theoretic and experimental studies on rosette-joint in cold-formed steel members", Dissertation, Nanjing University of Technology.

Tang, Yang, Shen, Zuyan and Chen, Yiyi (1998), "Test and analysis of axially loaded short column with cold-formed welded section", *Structural Engineers,* **3**, 7-14.

Ucak, Alper and Tsopelas, Panos (2004), "A new innovative design concept: Thin-walled corrugated steel columns", *Proc. of the 3rd Int. Conf. on Earthquake Engineering.* Weiqing Liu, Fuh-Gwo Yuan and Peter C. Chang, Beijing, Intellectual Property Publishing House and China Water Power Press. 566-571.

Yong, Ben and Yan, Jintang (2002), "Finite element in analysis and design of fixed-ended plain channel columns", *Finite Element Analysis and Design*, **38**, 549-566.

Yu, Wei-wen (2000), *Cold-Formed Steel Design*, 3rd Edition, John Wiley & Sons Inc.